Arif Hussain[1] and Gelli Ravikumar[1]

[1]Affiliation not available

January 31, 2025

Physics-Informed Intelligent Islanding Detection Method (PI-IIDM) for Cyber-Physical Networked DER-Microgrids

Arif Hussain, *Member, IEEE* , Gelli Ravikumar, *Sr. Member, IEEE*

***Abstract*—With the increasing integration of distributed energy resources (DER) into the distributed power system, the security of the power system from cyber-attacks is paramount. Cyber attacks make unintentional islanding detection challenging within the networked DER-integrated microgrid system. This study proposes a physics-informed approach for feature extraction and dimension reduction, leveraging principles from physics and domain-specific knowledge to analyze three-phase voltage and current signals. Moreover, a recurrent neural network (RNN) based gated recurrent unit (GRU), is introduced to fortify networked DER-integrated microgrids against cyber-physical threats, particularly focusing on unintentional islanding triggered by cyber-attacks at the point of common coupling (PCC). The most essential and difficult stage in an intelligent islanding detection system (IIDM) is feature extraction and selection, for which a physics-informed wavelet scattering network (WSN) and minimum redundancy maximum relevance (MRMR) algorithm are proposed. The WSN facilitates enhanced signal representation by capturing low and high-frequency information simultaneously, ensuring translation-invariant and deformation-stable signal representations. The MRMR algorithm is applied for dimension reduction, ensuring that the reduced feature space retains the most informative and physically relevant features while minimizing redundancy. Finally, GRU network is proposed for islanding detection. We developed an API integrated with RT-Lab to generate a diverse dataset for islanding, faults, and non-islanding scenarios to gather PCC voltage and current signals. The proposed method is assessed under various islanding, faults, and non-islanding scenarios, also considering the non-detection zone (NDZ), a critical factor affecting islanding conditions using an OPAL-RT real-time digital simulator. The proposed method is also validated using accuracy, selectivity, and sensitivity performance indices, demonstrating the effectiveness of physics-informed feature extraction/selection and GRU-based islanding detection (PI-IIDM), ensuring accurate islanding detection.**

***Index Terms*—Distributed Network, Gated Recurrent Unit, Islanding Detection, Power System, Wavelet Scattering Network.**

I. Introduction

Distributed energy resources (DERs) offer significant advantages over traditional power system networks, resulting in increased interest as a consequence of energy market deregulation, capital investment, the requirement for dependable and improved power quality (PQ), and environmental impacts. Electricity generation in a traditional electrical power system is centralized and distributed to consumers via transmission and distribution networks. Aside from the paybacks and leads, DER integration presented additional problems and faults in the power system, including inadvertent islanding caused by unintentional tripping of the main utility's circuit breaker (CB). Personnel safety, overvoltage, reconnection out of phase, PQ, and equipment protection are the key concerns associated with inadvertent islanding [1]. According to IEEE 1547-2018, islanding should be identified within 2 seconds to avoid the hazards associated with unintentional islanding [2].

Researchers have investigated the unintended challenge of islanding detection throughout the previous decade. Research continues; in the literature, various islanding detection methods (IDMs) are reported, with three fundamental categories: local, remote, and intelligent methods [3]. Remote methods need a communication interface and, due to their complexity and expensive cost, are reliable for big systems but not viable for small systems [4]. Local methods are further classified as active, passive, and hybrid. Active methods have noise and PQ problems due to external disturbance injection [5], while passive islanding methods have challenges with the non-detection zone (NDZ) and low speed, [6]. Hybrid methods integrate active and passive methods, have a long detection time, and are complicated to implement [7]. The state-of-art intelligent methods are gaining popularity as flaws and pitfalls in local and remote schemes become more apparent. The absence of threshold settings, no noise and PQ issues, low NDZ, fast speed, and minimal communication channel intervention are all advantages of intelligent IDMs, making intelligent methods more trustworthy and acceptable [1].

Signal and system (SnS) approaches have been used to improve the performance of passive methods in the literature because of their variety, stability, and simplicity of adaptation. Fourier transform (FT), S-transform, Hilbert Huang transform, wavelet transform (WT), and time-time-transform are the main signal processing methods for islanding detection. The required features are retrieved from the input signal and compared to a threshold value in signal processing-based passive IDMs. It is quite tough to choose a threshold value. To overcome this issue SnS approaches are combined with intelligent methods for extracting hidden features. Various studies are proposed for islanding detection using SnS with the machine and deep learning methods in [8], [9], [10], [11].

Numerous SnS approaches still need to be employed in electric power systems, particularly for islanding detection. Wavelet scattering networks (WSN) are one of them; they

"This research is funded partly by US NSF Grant CNS 2105269 and US DOE CESER Grant DE-CR000016."

Arif Hussain and Gelli Ravikumar are with the Department of Electrical and Computer Engineering, Iowa State University, USA. (e-mail: hussain@iastate.edu, and gelli@iastate.edu

perform admirably compared to FT and WT because of their multiscale contraction, linearization, and sparse representation properties [12]. Recurrent neural networks (RNNs) have emerged as powerful tools in various scientific and technological realms, yet their application in islanding detection remains underexplored. This study addresses this gap by proposing a novel solution integrating physics-informed mathematical signal processing techniques with RNN algorithms to bolster islanding detection capabilities. The focus lies on enhancing the resilience of networked DER-integrated microgrids against cyber-physical threats, particularly unintended islanding stemming from cyber attacks targeting the PCC. Motivated by gaps identified in existing literature, this work introduces a physics-informed intelligent islanding detection method (PI-IIDM) leveraging a WSN for feature extraction, MRMR for feature selection and a GRU for accurate islanding detection. The proposed PI-IIDM is rigorously evaluated using a cyber-physical networked DER-integrated microgrid test system, ensuring its effectiveness in real-world scenarios. Drawing insights from an extensive literature review, this study emphasizes the critical need for robust feature extraction and classification methods to achieve accurate detection, minimize the NDZ, and enable swift detection times, enhancing microgrid operations' reliability and security.

The key contributions of the WSN-GRU-based proposed PI-IIDM are:

- In the proposed PI-IIDM, unintentional islanding detection caused by cyber attacks on networked DER integrated microgrid is presented, focusing on V2G-enabled EVCS, PV, and BSS.
- In this study, a physics-informed mathematical signal processing method, WSN, is employed to extract hidden features from a voltage and current signal, introducing a novel approach to enhance feature representation.
- Dimension reduction using the MRMR method ensures that the reduced feature space retains the most informative and physically relevant features while minimizing redundancy.
- In this study, the cutting-edge recurrent algorithm GRU is used to identify islanding, faults, and non-islanding scenarios using physics-informed feature extraction and selection.
- Rigorous testing involves creating diverse scenarios using API integrated with RT-Lab to establish the robustness of the proposed PI-IIDM, providing comprehensive validation of its performance across various operational scenarios.
- Finally, the effectiveness of the proposed PI-IIDM is assessed according to several indicators such as accuracy, selectivity, sensitivity, and NDZ, ensuring a thorough evaluation of its capabilities and reliability.

II. Architecture of DER Integrated Microgrid

The architectural diagram in Fig. 1 illustrates a networked DER integrated microgrid, emphasizing communication and power infrastructures, alongside potential cyber threats at the PCC between the transmission and distribution (T&D) system and the microgrid. The T&D system represents the

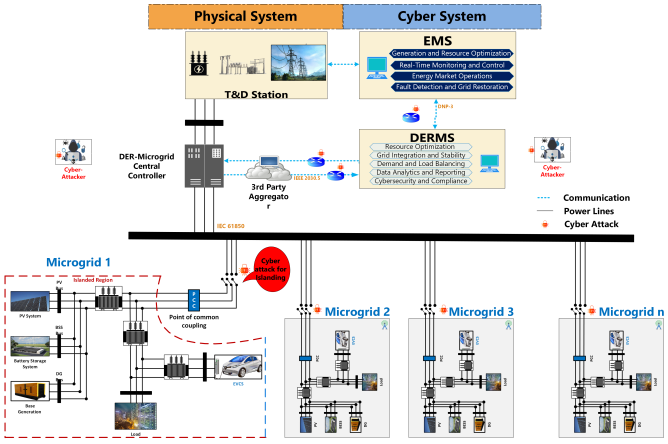

Fig. 1. Architecture of networked DER integrated microgrid

larger power transmission and distribution grid framework, including high-voltage lines and substations. The PCC is a critical interface facilitating power exchange between the microgrid and the main grid. It exposes it to cyber attacks, which could compromise the microgrid's stability and security, potentially leading to unintentional islanding. The microgrid consists of diverse DERs such as solar panels, wind turbines, batteries, loads, and an EVCS, collectively enabling localized power generation, storage, and consumption. Communication infrastructure is depicted as essential for real-time monitoring, control, and coordination within the microgrid. Moreover, the power infrastructure ensures efficient energy transfer and utilization, while the energy management system (EMS) and distributed energy management system (DERMS) govern resource optimization and dispatch. This study proposes a solution employing physics-informed mathematical signal processing and RNN algorithms for enhanced islanding detection, thereby fortifying the resilience of networked DER-integrated microgrids against cyber-physical threats, particularly focusing on unintentional islanding caused by cyber-attacks at the PCC.

III. Proposed PI-IIDM

The proposed physics-informed intelligent islanding detection method (PI-IIDM) method relies on extracting features, reducing dimensions, and employing an intelligent recurrent technique for detection. The proposed methodology, termed 'Physics-Informed Feature Extraction and Dimension Reduction,' integrates principles from physics and domain-specific knowledge into the computational process of analyzing three-phase voltage and current signals. Leveraging WSN for feature extraction, the approach captures essential signal characteristics rooted in signal processing and mathematical physics. Subsequently, MRMR is applied for dimension reduction, ensuring that the reduced feature space retains the most informative and physically relevant features while minimizing redundancy. This physics-informed process prioritizes features that align with the underlying physics of electrical signals. Furthermore, the methodology incorporates a GRU network for detecting islanding events, enabling enhanced understanding and modeling capabilities in electrical engineering applications.

WSN extracts features from complicated time-series data, focusing on 3-phase voltage and current signals collected from

a Simulink microgrid model. Our approach intends to improve signal representation while maintaining important information across several scales by using the inherent advantages of wavelet scattering, such as multiscale analysis, stability, and interpretability. The retrieved scattering characteristics were created with noise resistance, deformation invariance, and suitability for further machine learning tasks in mind. This method allows us to effectively handle the issue of feature engineering in the context of microgrid monitoring while enhancing the precision and interpretability of the PI-IIDM we have proposed.

Following feature extraction, we use the MRMR approach to efficiently lower the derived feature matrix's dimensionality. Due to its capacity to optimize feature relevance to the target variable while avoiding redundancy between selected features, the MRMR algorithm has significant significance in feature selection. MRMR enhances model generalization and resilience by choosing highly pertinent characteristics for the job while reducing information overlap. This strategy improves the effectiveness of our proposed method and the efficiency of the following processing stages by allowing the algorithm to collect the most insightful and distinctive parts of the input. By reducing the computational load while retaining critical data using MRMR-driven dimension reduction, we aim to improve the accuracy and efficiency of the results in our PI-IIDM.

Finally, we proposed the GRU network to detect a DER-integrated microgrid's islanding, faults, and non-islanding conditions. Our proposed PI-IIDM is built around this clever use of sophisticated recurrent neural networks. The GRU network's skill perfectly matches the dynamic character of microgrid activity in capturing complex temporal connections in sequential data. We can effectively learn and model complicated patterns within the data using GRU, leading to better detection accuracy. The recurring nature of the GRU network further enhances the ability to discriminate between islanding events and normal grid operation, making it simpler to apply the prior context. This use of state-of-the-art technology highlights our dedication to innovation. It ensures that our suggested technique is well-prepared to handle real-world events with high accuracy and dependability. Combining feature extraction and dimension reduction techniques with the predictive capabilities of GRU successfully addresses the difficult problems of islanding detection in microgrids. The systematic process of these three steps of the proposed PI-IIDM is shown as a flowchart in Fig. 2.

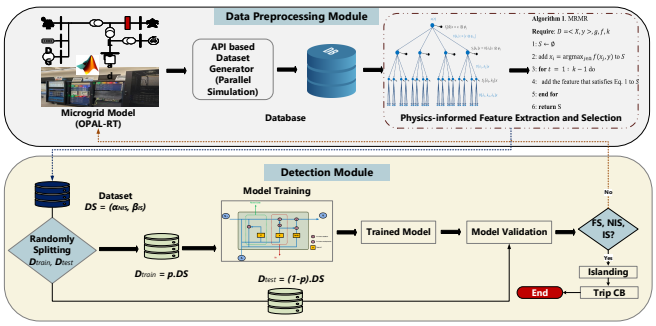

Fig. 2. Proposed WSN-GRU based PI-IIDM

A. Wavelet Scattering Network (WSN)

WSNs are convolution networks built on WT proposed by Mallat for invariant characterization using special wavelet methods for translation and rotation [13]. WSN is a wavelet-based enhanced time-frequency analysis technique. The procedure consists of an iterative complicated wavelet transform, modulus operation, and low-pass filtering averaging method. It has the advantages of translation invariance, local deformation stability, and rich feature information representation, as well as solving the problem of wavelet transform changing with time. The mother wavelet can be dilated and rotated to create a wavelet group.

$$\psi_{2^{-j}r}(t) = 2^{-dj}\psi(2^{-j}r^{-1}(t)) \tag{1}$$

where ψ is the mother wavelet, 2^j represents the dilation rate and is the rotation coefficient. The wavelets $\psi_{2^{-j}r}(t)$ act as band-pass filters to acquire signal components through convolution computation.

$$W_\lambda x = x * \psi_\lambda = \int x(\tau)\psi_\lambda(t-\tau)d\tau \tag{2}$$

where $\lambda = 2^{-j}r$, W_λ represents the wavelet transform operator and $*$ denotes the convolution computation. The scattering propagator of WSNs is created by iterating on the wavelet transform and modulus operators.

$$U_\lambda x = |W_\lambda x| = |x * \psi_\lambda| \tag{3}$$

$$U[p] = U_{\lambda_m} \dots U_{\lambda_2} U_{\lambda_1} \tag{4}$$

$$U[p]x = |x * \psi_{\lambda_1}| * \psi_{\lambda_1}| \dots \psi_{\lambda_m}| \tag{5}$$

where ψ_{λ_i} is the comprehensive operator and $U[p]$ is the scattering propagator incorporating the wavelet transform and modulus. Convolution with a scaled spatial window is now used to determine the low-frequency components.

$$\phi_j(t) = 2^{-dj}\phi(2^{-j}t) \tag{6}$$

$$S_j[p]x = |x * \psi_{\lambda_1}| * \psi_{\lambda_1}| \dots | * \psi_{\lambda_m}| * \phi_j \tag{7}$$

where ϕ is the initial scaling function, which at scale 2^j may be transformed to ϕ_j, and $S_j[p]$ is the propagator to extend the frequency scale. The WSNs can be constructed as illustrated in Fig. 3, by constantly computing Equations (5) and (7).

B. Minimum Redundancy Maximum Relevance (MRMR)

Peng et al. [14] first proposed the MRMR approach for pattern categorization systems that employ mutual information to assess relevance and redundancy. Following that, other versions of the MRMR technique were created. The MRMR feature selection method, which seeks to obtain the highest classification performance by decreasing redundancy among the selected features and increasing their relevance to the target class, has recently been widely utilized in various research domains. Most feature selection algorithms focus solely on the connection between features and classification categories, ignoring the interplay between features. Instead, the MRMR

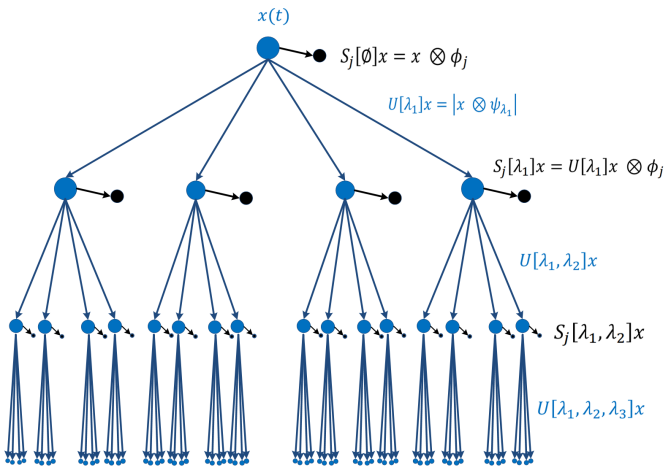

Fig. 3. A three-layer wavelet scattering network

feature selection method considers the quantity of information these features give for categorical characteristics and the impact of feature interaction on classification. Algorithm 1 outlines the steps employed in the MRMR for dimension reduction.

Algorithm 1: Feature Selection using MRMR

1) Initialize an empty set of selected features: $S_{\text{sel}} = \{\}$.
2) For i in $1, 2, \ldots, n$ (where n is the total number of features):
   a) Compute the relevance $D(X_i, Y)$ for each feature X_i.
   b) Compute the redundancy $R(X_i, X_j)$ between each pair of features X_i and X_j.
   c) Calculate the MRMR criteria $S_{\text{mrmr}}(X_i, Y, S_{\text{sel}})$ for each feature X_i, combining relevance with negative redundancy and considering previously selected features S_{sel}.
3) Select the feature X_i that maximizes the MRMR criterion $S_{\text{mrmr}}(X_i, Y, S_{\text{sel}})$ in each iteration and add it to S_{sel}.
4) Repeat step 2 until the desired number of features is selected or until convergence.
5) Return the selected subset of features S_{sel} as the optimal feature set.

C. Gated Recurrent Unit (GRU)

A form of RNN called the GRU was created to overcome some drawbacks of conventional RNNs and LSTMs, including vanishing gradient issues and long-term dependencies [15]. Despite having comparable objectives, GRU offers certain benefits over LSTM regarding simplicity and computational effectiveness. For many sequential tasks, including classification issues, GRUs are often utilized. GRU does this by including gating mechanisms that enable the network to manage the information flow over time. In contrast to LSTM's three gating mechanisms (input gate, output gate, and forget gate), GRU only utilizes two (update gate and reset gate), making it theoretically simpler than LSTM. GRU is less complicated than LSTM, which makes it simpler to comprehend, use, and train. In comparison to LSTM, GRU has a more direct information flow conceptually. In an LSTM, the input and output gates regulate the information flow, while the forget gate explicitly determines how much of the prior hidden state should be forgotten. On the other hand, in GRU, the reset gate affects the candidate's activation, while the update gate determines how much of the prior concealed state should be kept. This simplification could make it easier for GRU to adjust to different sequential patterns.

Let's now examine the mathematical features of GRU and how they relate to the above-mentioned conceptual advantages:

The update gate z_t in GRU controls the trade-off between the previous hidden state h_{t-1} and the candidate activation h'_t:

$$z_t = \sigma(W_z \cdot [h_{t-1}, x_t]) \tag{8}$$

where W_z is the weight matrix for the update gate, σ is the sigmoid activation function, h_{t-1} is the previous hidden state and x_t is the current input at time step t.

The reset gate r_t determines how much of the previous hidden state h_{t-1} is forgotten when computing the new candidate activation h'_t:

$$r_t = \sigma(W_r \cdot [h_{t-1}, x_t]) \tag{9}$$

where W_r is the weight matrix for the reset gate.

The candidate activation h'_t represents the new candidate values for the hidden state at time step t:

$$h'_t = \tanh(W_h \cdot [r_t \odot h_{t-1}, x_t]) \tag{10}$$

where W_h is the weight matrix for the reset gate.

The current hidden state h_t is a combination of the previous hidden state h_{t-1} and the candidate activation h'_t controlled by the update gate z_t:

$$h_t = (1 - z_t) \odot h_{t-1} + z_t \odot h'_t \tag{11}$$

where h_{t-1} is the previous hidden state and h'_t is the candidate activation.

IV. Testbed Implementation

We consider a DER-integrated microgrid system network to demonstrate our proposed PI-IIDM as shown in Fig. 4. This DER-integrated microgrid consists of PV generation, a battery, loads, and a vehicle-grid-enabled electric vehicle (EV) charging station [16]. The selected microgrid model is implemented on the OP5600 OPAL-RT real-time digital simulator integrated with the hardware setup available at the PowerCyber [17] lab at Iowa State University. We integrate the model with the API and the ARTEMiS-SSN of the OPAL-RT. The battery will be utilized for solar smoothing, peak-shaving, and energy imbalance after the microgrid has been connected to the main grid. Following that, the PV inverters and batteries switch to grid-following mode. The PV inverter will function as follows when the microgrid is islanded. However, the battery inverter will function in grid-forming mode. The EVs' batteries may support both the electrical grid and the microgrid. Using Simscape Power Systems, the simulation models were created in MathWorks Simulink.

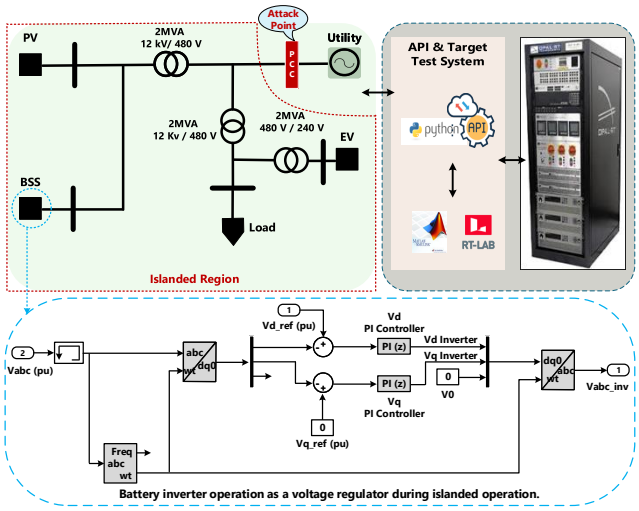

Fig. 4. DER integrated microgrid test system for the proposed IIDM

A. Preparation of Dataset for IIDM

We generated comprehensive datasets encompassing line faults during non-islanding, including single line (SL), SL-ground (SLG), double line (DL), DLG, 3-phase (TL), and TLG faults. For switching scenarios during non-islanding, we considered load switching and capacitor switching. We considered two scenarios for islanding: large and small power mismatch cases. These scenarios are modeled and generated using an automated API integrated with RT-lab in a MATLAB/Simulink environment. The performance of the proposed IIDM relies significantly on the abundant dataset. In contrast, it is important to observe the absence of a practical dataset comprising possible fault scenarios during non-islanding (α_{FS}), switching during non-islanding scenarios (β_{NIS}) and islanding scenarios (γ_{IS}). Therefore, it is inevitable to devise a systematic methodology to generate the dataset through our proposed auto data generation [18]. The dataset (DS) comprising α_{FS}, β_{NIS} and γ_{IS} for a considered network is defined as follows:

$$DS = f(\alpha_{FS}, \beta_{NIS}, \gamma_{IS}) \tag{12}$$

$$\alpha_{FS} = \{\alpha_{SL}, \alpha_{DLG}, ..., \alpha_{TLG}\} \tag{13}$$

$$\beta_{NIS} = \{\beta_{LS}, \beta_{CS}\} \tag{14}$$

$$\gamma_{IS} = \{\gamma_{LPM}, \gamma_{SPM}\} \tag{15}$$

To test the proposed method, 579 distinct cases were generated using the API, and the data is collected in the form of 3-phase voltage and 3-phase current at PCC. Out of which 200 cases for islanding, 194 cases for line faults under non-islanding conditions, and 185 cases for load and capacitor switching under non-islanding conditions to make a balanced and unbiased dataset. We consider α_{FS} = 195 scenarios, including all eleven types of line faults and six angles ranging from $(0 - 360)$. The fault resistance is also changed in the 0.01 to 1 ohms range. We consider β_{NIS} = 185 scenarios. In contrast, for β_{LS}, we considered 95 scenarios by changing a dynamic load with active power (P) $(5 - 50\text{kW})$ and reactive power (Q) variations $(0 - 4.5\text{kW})$, and for α_{CS}, which has 90 scenarios within the range of P $(0 - 450\text{W})$ and Q $(1 - 10\text{kW})$.

TABLE I
DATA GENERATION SCENARIOS FOR THE PROPOSED PI-IIDM

Scenarios	Ranges	Cases
	Line Faults during Non-Islanding	
SLG, DLG, TLG	R = $(0.01 - 1$ ohm) & $\theta = (0 - 360)$	194
	Switching during Non-Islanding	
Load Switch.	P = $(5 - 50\text{kW})$ & Q = $(0 - 4.5\text{kW})$	95
Capacitor Switch.	P = $(0 - 450\text{W})$ & Q = $(1 - 10\text{kW})$	90
	Islanding (γ_{IS})	
LPM	0 to $\pm 50\%$	170
SPM	0 to $\pm 5\%$	30

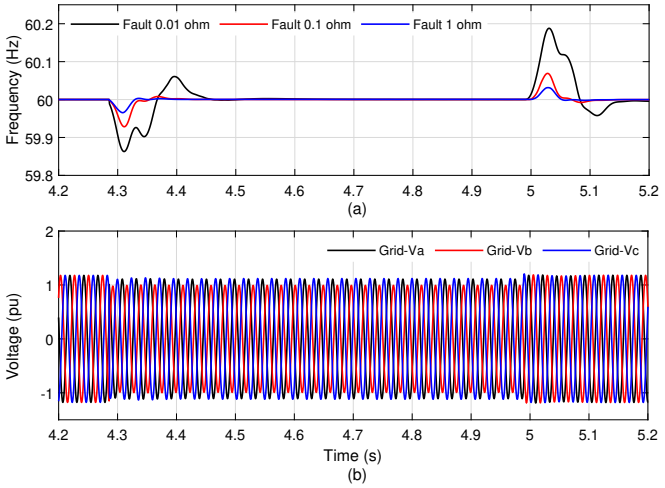

Fig. 5. Behavior during α_{FS} a) frequency with different fault resistance and b) grid voltage

For γ_{IS}, we incorporate two scenarios, large power mismatch (γ_{LPM}), and small power mismatch scenario (γ_{SPM}). The voltage data is extracted for γ_{LPM} scenarios by varying the active power between 0 to ±50%. The most important situation during islanding is the NDZ, and in this study, γ_{SPM} scenarios were considered within NDZ (±5%). Table 1 presents the summary of data generation for the proposed PI-IIDM.

V. Results and Discussion

A. Dynamics of Signals Across Faults, Non-Islanding, and Islanding Scenarios

Fig. 5 illustrates the frequency and voltage behavior during α_{FS}, revealing changes during α_{LF} at the initiation (4.4 sec) and conclusion (5 sec) of the fault. Fig. 5a illustrates the impact of line faults with different fault resistances. We can see that low-impedance faults have a higher impact than high-impedance faults, corresponding to the higher fault current and the associated effects on the grid. Conversely, Fig. 5b illustrates the voltage behavior across the three-phase grid, showcasing a decline in voltage upon the incidence of faults.

The effects of β_{LS} and β_{CS} on frequency and voltage characteristics are further elucidated in Fig. 6. Fig. 6a analyzes the deviation in frequency during load and capacitor switching. It is observed that the impact of β_{LS} is notably heightened due to the sudden injection of dynamic load into the system. This abrupt addition of load alters the system's power balance, resulting in more pronounced frequency fluctuations. Additionally, Fig. 6b demonstrates the voltage response resulting

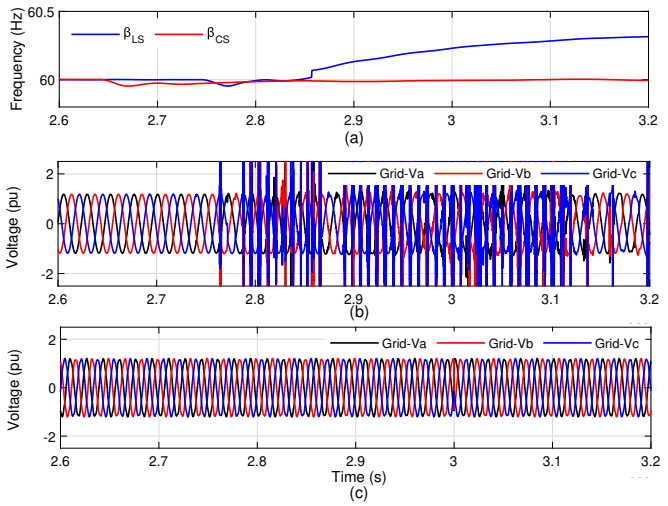

Fig. 6. Behavior during β_{NIS} a) frequency for β_{LS} and β_{CS} b) grid voltage during β_{LS} and c) grid voltage during β_{CS}

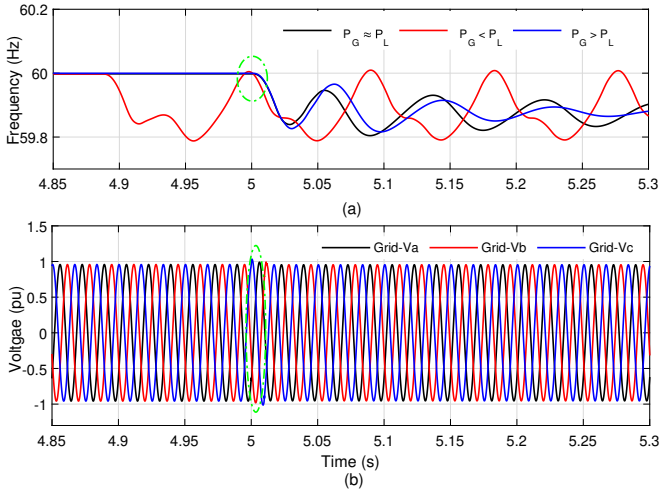

Fig. 7. Behavior during γ_{IS} a) frequency with γ_{LPM} and γ_{SPM} and b) grid voltage in γ_{SPM}

from the injection of a dynamic load, revealing a substantial impact characterized by the introduction of significant harmonics into the grid voltage waveform. These harmonics can lead to undesirable effects such as increased losses, interference with sensitive equipment, and reduced power quality. Finally, Fig. 6c depicts the voltage behavior during the injection of β_{CS}, offering insights into how capacitor switching events affect grid voltage stability and quality.

Two distinct islanding scenarios γ_{IS} are generated, as outlined in Table I. The proposed algorithm's performance is validated through simulations of all potential islanding instances. Furthermore, the algorithm is tested for its ability to identify islanding in numerous active and reactive power imbalances between load and generation within the islanded network. Traditional methodologies face challenges in recognizing islanding when there is a minimal difference between load and power generation, particularly in the region referred to as NDZ. We conducted simulations with γ_{SPM} scenarios within a range of ±5% to address this issue. The islanding scenario is triggered at 5 seconds by tripping the CB at the PCC. The BSS neither charges nor discharges. When the microgrid is unexpectedly islanded at t = 5 seconds, the

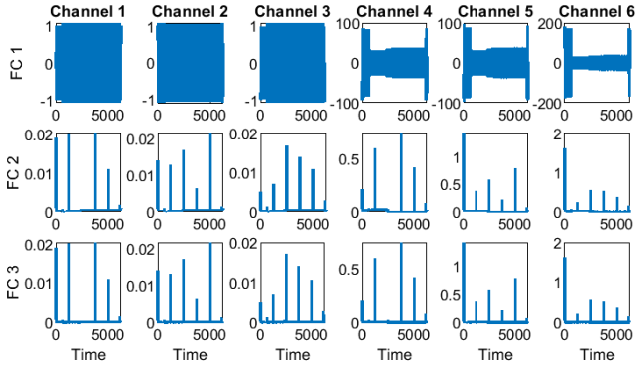

Fig. 8. Frequency components 1, 2, and 3 for 6 channels for α_{FS}

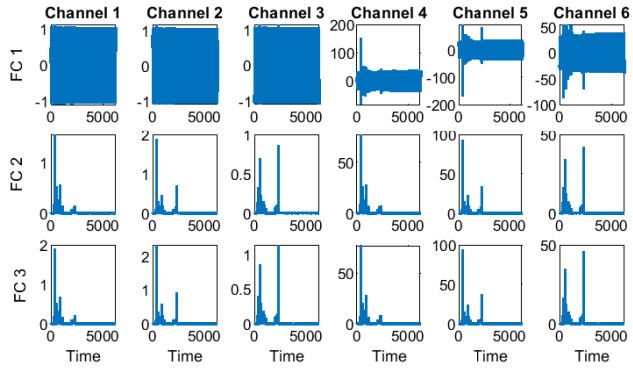

Fig. 9. Frequency components 1, 2, and 3 for 6 channels for β_{NIS}

BSS controller enters islanded mode to maintain the desired voltage and frequency. Frequency and voltage signals are closely monitored at PCC. The corresponding behaviors are depicted in Fig. 7. The changes in frequency signal behavior during γ_{SPM} where the black line shows the generation is nearly equal to load $P_G \approx P_L$, the red line graph shows $P_G < P_L$ +50% scenario of γ_{LPM}, and finally blue line $P_G > P_L$ that is -50% scenarios of γ_{LPM}. Fig. 7a shows that the frequency deviates less when the load is near to or less than the generation. Still, whenever the generation is smaller than the load, the frequency changes significantly, causing instability in the system, where the grid forming the BSS system tries to control the frequency and voltage stability. Fig. 7b shows the voltage behavior during islanding. It is evident that during γ_{SPM}, the difference between generation and load is either zero or near zero, and no significant changes are observed in the three-phase voltage. However, utilizing WSN, we were able to extract distinctive characteristics in the time-frequency representation of the voltage and current signals across all islanding situations.

B. WSN Feature Analysis

In our study, we embarked on a novel approach, leveraging the scattering transform methodology, to extract features from a dataset comprising six input features, each spanning a length of 100,000 samples. This unique methodology allowed us to gain deeper insights into the underlying characteristics of these input signals. The resulting features, organized into a structured representation, offered a comprehensive view of the input data's complexity and dynamics. Specifically, the scattering transform generated a feature set with dimensions

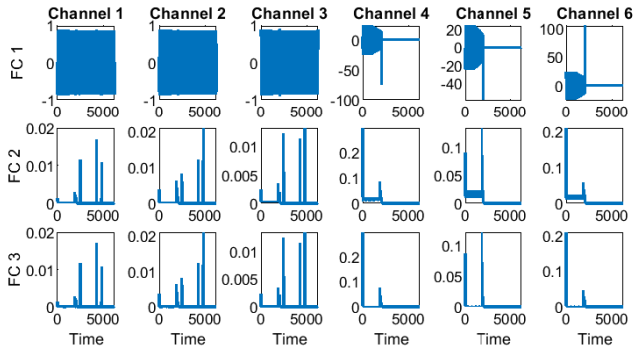

Fig. 10. Frequency components 1, 2, and 3 for 6 channels for γ_{IS}

of 56x6250x6, where the first dimension (56) captured various frequency components, the second dimension (6250) represented temporal variations over the length of the signals, and the third dimension (6) encapsulated different orders of scattering, elucidating hierarchical patterns within the data. This feature extraction process enabled us to obtain a rich and informative representation of the input features, paving the way for enhanced analysis and understanding within our research domain.

Fig. 8 through 10 display the initial three frequency components of each signal following the application of wavelet scattering for feature extraction. Each signal consists of three components for voltage and three for current. Channels 1, 2, and 3 correspond to the three-phase voltage, while channels 4, 5, and 6 pertain to the three-phase current. Analysis of Fig. 8, 9, and 10 reveals discernible differences in magnitude within the third frequency component, distinguishing between occurrences of α_{FS}, β_{NIS}, and γ_{IS}. In this context, each subplot in the figure corresponds to a specific combination of frequency component and channel. The horizontal axis represents time, while the vertical axis represents the magnitude of the frequency component. The six channels depict different scattering orders, capturing varying levels of abstraction and complexity in the signal representation. By visualizing these features, we gain insights into the underlying dynamics of the signal, facilitating quantitative analysis and interpretation across different scales and levels of detail.

C. Validation and Performance Evaluation

In the proposed PI-IIDM, the DS is split into D_{train} and D_{test} for the training and testing with a train-test split ratio of 80:20. To validate and evaluate the effectiveness of proposed PI-IIDM three performance indicies are utilized as defined below:

$$\text{Accuracy} = \frac{TP + TN}{TP + TN + FP + FN} \tag{16}$$

$$\text{Selectivity} = \frac{TN}{TN + FP} \tag{17}$$

$$\text{Sensitivity} = \frac{TP}{TP + FN} \tag{18}$$

Where: TP (True Positives): Instances correctly classified as $'IS'$. TN (True Negatives): Instances correctly classified as not $'IS'$ ($'FS'$ or $'NIS'$). FP (False Positives): Instances incorrectly classified as $'IS'$ when they are not. FN (False Negatives): Instances incorrectly classified as not $'IS'$.

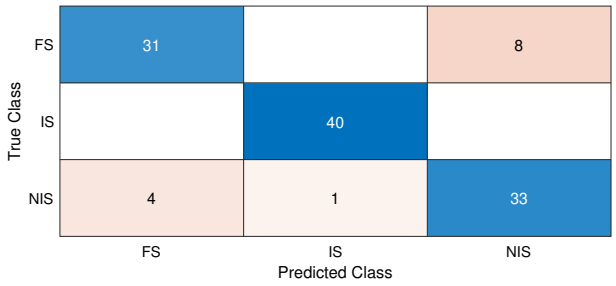

Fig. 11. Testing confusion metrics for the proposed PI-IIDM

Initially, the model underwent training using features extracted by the WSN for feature extraction. Subsequently, the proposed MRMR model was applied for feature selection, following the steps outlined in Algorithm 1. As summarized in Table II, the outcomes of training the GRU network were compared between utilizing the original WSN features and employing MRMR-selected features. Analysis of Table II indicates that the MRMR feature selection approach yields notable accuracy, selectivity, sensitivity, and training duration improvements. Particularly noteworthy is the significant reduction in training time achieved through dimension reduction and feature selection techniques.

TABLE II
TESTING RESULTS BEFORE AND AFTER DIMENSION REDUCTION

Data	Performance Indices			
	Accuracy	Selectivity	Sensitivity	Training Time
WSN Features	82.74%	97.29%	90.00%	02:43:53
MRMR Features	89.03%	97.56%	100.0%	00:05:28

Fig. 11 shows the confusion matrix of the proposed model with the testing dataset in this context. Our model's primary goal is to identify islanding events reliably, and the outcomes look promising. The confusion matrix illustrates how the proposed approach achieves a high selectivity rate of 97.56% with only one FP event and adequately identifies all TP events, resulting in a sensitivity of 100%. In addition, Fig. 12 presents a graphical depiction of the outcomes, with the actual class represented by blue and the predicted class represented by red. Green dotted rectangles show misclassification cases. Our proposed approach performs better, as demonstrated by its high selectivity rates and ability to detect islanding events with few false positives and negatives. Furthermore, the graphical depiction makes the model's performance easy to understand and allows for more research into how well it can differentiate between various classes.

Furthermore, unlike other IDMs based on thresholds and the injection of disturbances, this technique does not need any threshold values to distinguish between islanding and other scenarios, even when there is almost zero power mismatch between generation and load, also known as NDZ. In the proposed PI-IIDM, 30 γ_{SPM} cases are considered to validate the NDZ for the proposed PI-IIDM. The proposed method's selectivity and sensitivity indicate minimum NDZ as it only has one FP out of 40 events. Furthermore, Fig. 13 provides

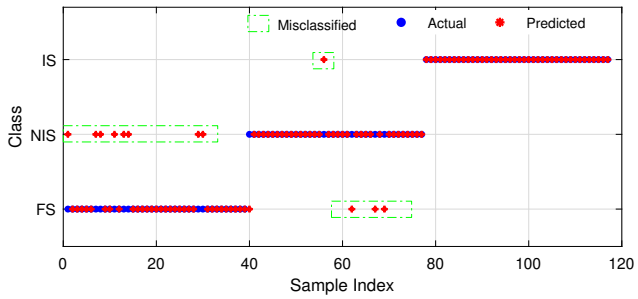

Fig. 12. Predicted vs actual classes with misclassified scenarios

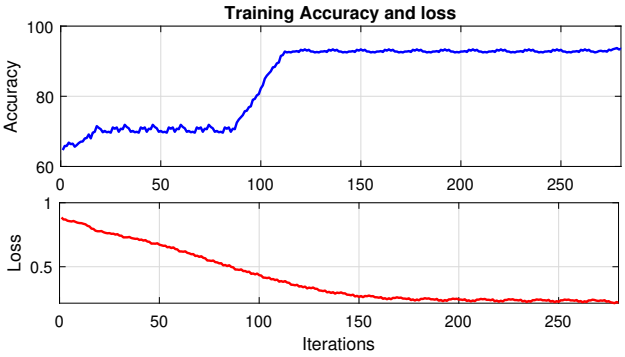

Fig. 13. Training accuracy and loss for proposed GRU network

a visual representation of the model's accuracy and loss progression, demonstrating the efficacy of our method for islanding detection. Interestingly, the results show that the expected outcomes for islanding detection are reached in less than 20 epochs.

VI. Conclusion

In this study, we proposed a PI-IIDM tailored for networked DER-integrated microgrids. Our physics-informed approach leverages WSN and MRMR algorithms for feature extraction and dimension reduction with a GRU network for detection. Our proposed PI-IIDM offers a novel approach to accurately detect islanding, faults, and non-islanding scenarios in the DER-integrated microgrid systems. Our methodology begins by extracting translation-invariant and deformation-stable signal representations through wavelet convolution cascades, incorporating nonlinear modulus operations and averaging operators within the WSN framework. We employ MRMR for dimension reduction to enhance efficiency. Subsequently, the GRU is trained to discern islanding events based on these refined features, utilizing voltage and current signals acquired at the PCC. Simulations conducted on an OPAL-RT real-time digital simulator confirm the efficacy of our WSN-GRU-based IIDM. Noteworthy advantages of our approach over existing methods include:

- Accurate detection of unintentional islanding events caused by cyber-attacks in networked DER-integrated microgrids achieving a sensitivity of 100%.
- Elimination of threshold dependencies inherent in passive methods, circumventing the need for external disturbance injection as required by active methods, and obviating the necessity of communication interfaces inherent in remote methods.
- Integration of feature extraction and dimension reduction techniques with the discriminative capabilities of GRU, effectively addressing the complexities of islanding detection in networked DER-integrated microgrids amidst cyber-physical threats.
- Comprehensive validation of the proposed IIDM's performance across diverse operational scenarios, achieved through rigorous testing facilitated by API integration with RT-Lab, ensuring robustness under both islanding and non-islanding conditions.

References

[1] A. Hussain, C.-H. Kim, and A. Mehdi, "A comprehensive review of intelligent islanding schemes and feature selection techniques for distributed generation system," *IEEE Access*, vol. 9, pp. 146 603–146 624, 2021.

[2] D. G. Photovoltaics and E. Storage, "Ieee standard for interconnection and interoperability of distributed energy resources with associated electric power systems interfaces," *IEEE Std*, vol. 1547, pp. 1547–2018, 2018.

[3] A. Hussain, A. Mehdi, and C.-H. Kim, "A communication-less islanding detection scheme for hybrid distributed generation systems using recurrent neural network," *International Journal of Electrical Power & Energy Systems*, vol. 155, p. 109659, 2024.

[4] K.-L. Chen, Y. Guo, J. Wang, and X. Yang, "Contactless islanding detection method using electric field sensors," *IEEE Transactions on Instrumentation and Measurement*, vol. 70, pp. 1–13, 2020.

[5] S. Murugesan and V. Murali, "Active unintentional islanding detection method for multiple-pmsg-based dgs," *IEEE Transactions on Industry Applications*, vol. 56, no. 5, pp. 4700–4708, 2020.

[6] C. R. Reddy, J. H. Choi, B. Pangedaiah, and S. V. R. Reddy, "Absolute positive sequence voltage difference based passive islanding detection in micro grids," *IEEE Transactions on Industry Applications*, 2024.

[7] T. Peng, C. Bai, X. Song, and S. Duan, "An islanding detection method based on the reactive power disturbance for multiple inverter-based dg systems," *IEEE Transactions on Industrial Electronics*, 2023.

[8] M. Mishra and P. K. Rout, "Loss of main detection in distribution generation system based on hybrid signal processing and machine learning technique," *International Transactions on Electrical Energy Systems*, vol. 29, no. 1, p. e2676, 2019.

[9] Y. Wang, J. Ravishankar, and T. Phung, "Wavelet transform-based feature extraction for detection and classification of disturbances in an islanded micro-grid," *IET Generation, Transmission & Distribution*, vol. 13, no. 11, pp. 2077–2087, 2019.

[10] S. K. Manikonda and D. N. Gaonkar, "Idm based on image classification with cnn," *The Journal of Engineering*, vol. 2019, no. 10, pp. 7256–7262, 2019.

[11] A. A. Abdelsalam, A. A. Salem, E. S. Oda, and A. A. Eldesouky, "Islanding detection of microgrid incorporating inverter based dgs using long short-term memory network," *IEEE Access*, vol. 8, pp. 106 471–106 486, 2020.

[12] Y. M. Keerthana, M. K. Reddy, P. Alku, K. S. Rao, and P. Mitra, "Automatic classification of neurological voice disorders using wavelet scattering features," *Speech Communication*, p. 103040, 2024.

[13] J. Andén and S. Mallat, "Deep scattering spectrum," *IEEE Transactions on Signal Processing*, vol. 62, no. 16, pp. 4114–4128, 2014.

[14] H. Peng, F. Long, and C. Ding, "Feature selection based on mutual information criteria of max-dependency, max-relevance, and min-redundancy," *IEEE Transactions on pattern analysis and machine intelligence*, vol. 27, no. 8, pp. 1226–1238, 2005.

[15] R. Dey and F. M. Salem, "Gate-variants of gated recurrent unit (gru) neural networks," in *2017 IEEE 60th international midwest symposium on circuits and systems (MWSCAS)*. IEEE, 2017, pp. 1597–1600.

[16] C. Keerthisinghe and D. S. Kirschen, "1 real-time digital simulation of microgrid control strategies," in *2020 IEEE Power & Energy Society Innovative Smart Grid Technologies Conference (ISGT)*. IEEE, 2020, pp. 1–5.

[17] G. Ravikumar, B. Hyder, and M. Govindarasu, "Hardware-in-the-loop cps security architecture for der monitoring and control applications," in *2020 IEEE Texas Power and Energy Conference (TPEC)*. IEEE, 2020, pp. 1–5.

[18] A. A. Mantha, A. Hussain, and G. Ravikumar, "Hil testbed-based auto feature extraction and data generation framework for ml/dl-based anomaly detection and classification," in *2024 IEEE Power & Energy Society Innovative Smart Grid Technologies Conference (ISGT)*. IEEE, 2024, pp. 1–5.